








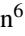

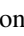






# Mars from the InSight: Seismology Beyond Earth

Brigitte Knapmeyer-Endrun<sup>1</sup>  , W. Bruce Banerdt<sup>2</sup> , Suzanne E. Smrekar<sup>2</sup> ,  
Philippe Lognonné<sup>3</sup> , Domenico Giardini<sup>4</sup> , Caroline Beghein<sup>5</sup> ,  
Éric Beucler<sup>6</sup> , Ebru Bozdağ<sup>7</sup> , John Clinton<sup>4</sup> , Raphael F. Garcia<sup>8</sup> ,  
Jessica C. E. Irving<sup>9</sup> , Taichi Kawamura<sup>3</sup> , Sharon Kedar<sup>2</sup> ,  
Ludovic Margerin<sup>10</sup> , Mark P. Panning<sup>2</sup> , Tom W. Pike<sup>11</sup> ,  
Ana-Catalina Plesa<sup>12</sup> , Nicholas Schmerl<sup>13</sup> , Nicholas Teanby<sup>8</sup> ,  
Renee Weber<sup>14</sup> , Mark Wieczorek<sup>15</sup> , Salma Barkaoui<sup>3</sup> , Nienke Brinkman<sup>4</sup> ,  
Savas Ceylan<sup>4</sup> , Constantinos Charalambous<sup>11</sup> , Nicolas Compaire<sup>8</sup> ,  
Nikolaj Dahmen<sup>4</sup> , Martin van Driel<sup>4</sup> , Anna Horleston<sup>9</sup> , Quancheng Huang<sup>7</sup> ,  
Kenneth Hurst<sup>2</sup> , Balthasar Kenda<sup>3</sup> , Amir Khan<sup>4,16</sup> , Doyeon Kim<sup>4</sup> ,  
Martin Knapmeyer<sup>12</sup> , Jiaqi Li<sup>5</sup> , Sabrina Menina<sup>3</sup> , Naomi Murdoch<sup>8</sup> ,  
Clément Perrin<sup>6</sup> , Martin Schimmel<sup>17</sup> , Simon C. Stähler<sup>4</sup> ,  
and Eléonore Stutzmann<sup>3</sup> 

<sup>1</sup> Bensberg Observatory, University of Cologne, Vinzenz-Pallotti-Str. 26, 51429 Bergisch Gladbach, Germany

bknapmey@uni-koeln.de

<sup>2</sup> Jet Propulsion Laboratory, California Institute of Technology, Pasadena, CA 91109, USA

<sup>3</sup> Université de Paris Cité, Institut de Physique du globe de Paris, CNRS, 75005 Paris, France

<sup>4</sup> Institute of Geophysics, ETH Zurich, Sonneggstr. 5, 8092 Zurich, Switzerland

<sup>5</sup> Department of Earth, Planetary, and Space Sciences, University of California, 595 Charles Young Drive East, Box 951567, Los Angeles, CA 90095-1567, USA

<sup>6</sup> Laboratoire de Planétologie et Géodynamique, UMR6112, Univ. Nantes, Univ. Angers, CNRS, 2 rue de la Houssinière - BP 92208, 44322 Nantes Cedex 3, France

<sup>7</sup> Department of Geophysics, Colorado School of Mines, 1500 Illinois Street, Golden, CO 80401, USA

<sup>8</sup> Institut Supérieur de l'Aéronautique et de l'Espace SUPAERO, 10 Avenue Edouard Belin, 31400 Toulouse, France

<sup>9</sup> School of Earth Sciences, University of Bristol, Wills Memorial Building, Queens Road, Bristol BS8 1RJ, UK

<sup>10</sup> Institut de Recherche en Astrophysique et Planétologie, Université Toulouse III Paul Sabatier, CNRS, CNES, 14 Av. E. Belin, 31400 Toulouse, France

<sup>11</sup> Department of Electrical and Electronic Engineering, Imperial College London, South Kensington Campus, London SW7 2AZ, UK

<sup>12</sup> Institute of Planetary Research, German Aerospace Center (DLR), 12489 Berlin, Germany

<sup>13</sup> College Park, Department of Geology, University of Maryland, 8000 Regents Dr., College Park, MD 20782-4211, USA

<sup>14</sup> NASA MSFC, NSSTC Mail Code ST13, 320 Sparkman Drive, Huntsville, AL 35805, USA

<sup>15</sup> Laboratoire Lagrange, Université Côte d'Azur, Observatoire de la Côte d'Azur, CNRS, Nice, France

<sup>16</sup> Institute of Theoretical Physics, University of Zürich, Winterthurerstr. 190, 8057 Zürich, Switzerland

<sup>17</sup> Geosciences Barcelona – CSIC, Barcelona, Spain

© The Author(s), under exclusive license to Springer Nature Switzerland AG 2022

R. Vacareanu and C. Ionescu (Eds.): ECEES 2022, SPEES, pp. 74–89, 2022.

[https://doi.org/10.1007/978-3-031-15104-0\\_5](https://doi.org/10.1007/978-3-031-15104-0_5)

**Abstract.** When NASA's InSight lander touched down in Elysium Planitia, Mars, in November 2018 and deployed its seismometer SEIS, it ushered in a new age for planetary seismology - more than 40 years after the first attempt to record marsquakes with the Viking missions. SEIS, an extremely sensitive instrument, has by now provided near continuous seismic records for more than 3 years. Its rich dataset shows Mars to be seismically active, with over 1,300 marsquakes detected so far, mostly with magnitudes below 4. Despite their small size, these quakes provide important and unprecedented constraints on the interior structure of the planet, from the shallow subsurface via the crust, the lithosphere, and the mantle transition zone down to the core, and allow to study Martian tectonics and thermo-chemical evolution. Single-station seismology has answered some of the big questions about the interior of our planetary neighbour, and this contribution gives an overview of results and surprises so far.

**Keywords:** Seismology · Mars · Interior structure

## 1 Introduction

### 1.1 A planet's Interior from Seismology

When seismic waves traverse a planetary body, they gather information on the media they travel through on their way. The ability to extract this information from seismograms has allowed seismology to play a major role in constraining the interior structure of planet Earth, including the variable thickness and structure of the crust, the depth of phase transitions in the mantle, and the state and size of the outer and inner core. While interior models get more and more refined for Earth and focus on 3D or even 4D (spatial and temporal) variations, comparable knowledge for other planets is much more limited. This impedes our understanding of the thermal and geodynamical evolution of terrestrial planets in general, including the prerequisites required for and significance of a geodynamo and plate tectonics. Comparative planetology is an important tool to understand the Earth, its uniqueness in the Solar System, and how it became what it is.

Seismology was an integral part of the initial scientific exploration of the Moon, from three seismometers on the unmanned Ranger missions in 1962, none of which managed a successful lunar landing [1], to the seismometers deployed by the astronauts of Apollo 11, 12, 14, 15 and 16 between 1969 and 1972 that recorded thousands of moonquakes during eight years of operation [2]. Most recorded moonquakes belong to a type of seismicity unknown on Earth: deep moonquakes forming clusters at 800 to 1100 km depth in the lunar mantle that are periodically active, depending on tidal stresses [3]. The Apollo seismic data allowed to constrain the Moon's crustal thickness, the velocity structure of the mantle, and the size and state of the lunar core [for a recent summary, see 4].

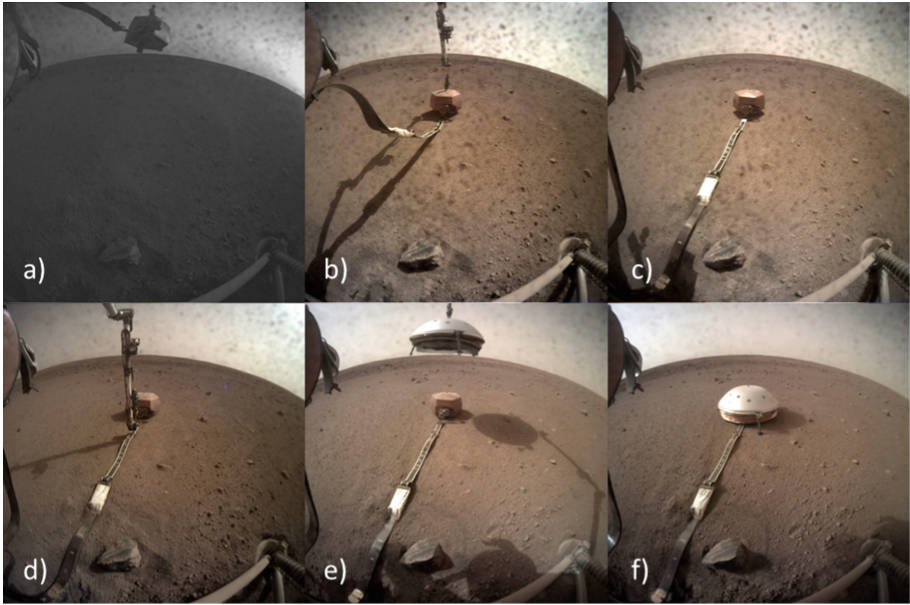
After the success of the Apollo passive seismic experiments, seismometers were also included in the next step of the exploration of the solar system, i.e. the two Viking landers going to Mars in 1976. Being the first landed missions to Mars, they were designed to investigate many different scientific questions about our neighboring planet, seismology not being a priority. The short-period seismometers on each of the Viking landers were thus placed in a less-than-ideal location, i.e. on the lander deck about 1 m above ground, and data transmission was severely constrained [5]. The Viking I seismometer failed to uncage and thus to record any meaningful data, but Viking II registered more than 500 Martian days (“sols”) of seismic data. However, due to the location of the sensor on the lander deck, those data were heavily contaminated by wind [6], and after analysis, only one possible, but unconfirmed, seismic event remained within this data set [5].

This result somewhat dampened the enthusiasm for extraterrestrial seismology, and it took more than 40 years and numerous efforts to send another seismometer to Mars on NASA’s InSight (Interior Exploration using Seismic Investigations, Geodesy and Heat Transport) mission in 2018. Based on the Viking experience, InSight was the first mission to remotely deploy a seismometer on the surface of an extraterrestrial body with the help of a robotic arm [7], a procedure that took almost three months to accomplish (Fig. 1). The seismometer, SEIS (Seismic Experiment for Internal Structure), is a highly sensitive six-axes sensor, consisting of a three-component very broad-band (VBB) and a three-component short-period (SP) seismometer [8].

## 1.2 Knowledge on the Interior of Mars Prior to InSight

Early on, Mars as a terrestrial planet was expected to have undergone similar processes of accretion and differentiation as Earth, resulting in a buoyant crust, a silicate mantle, and an iron-rich metallic core [9]. However, the exact thickness of these layers and details on their properties were not well known before InSight, as summarized by [10]: Orbital measurements of gravity and topography can accurately constrain relative variations in crustal thickness, but rely on assumptions on crustal and mantle densities and the minimum crustal thickness. Depending on these assumptions, and not considering any lateral variations in crustal density, average crustal thickness estimates for Mars varied between 39 and 110 km, with no information on internal structure or layering of the crust.

Likewise, estimates for the lithospheric thickness of Mars had been based on gravity and topography as well as deflection due to polar ice cap loading, resulting in estimates for the elastic lithospheric thickness of more than 150 km, and more than 300 km beneath the north polar cap. Depending on composition and areotherm, the seismic velocity of the mantle could a priori only be constrained to within  $\pm 1$  km/s.



**Fig. 1.** Robotic deployment of SEIS on the surface of Mars as witnessed by InSight’s Instrument Context Camera (ICC). The instrument deployment arm (IDA) lifted SEIS off the lander deck (a) and put it on the ground at a location selected based on analysis of photos of the landing site (b). Afterwards, the tether was dropped (c) and, after leveling SEIS close to the ground, adjusted via the pinning mass with the IDA (d). Finally, the IDA deployed the Wind and Thermal Shield (WTS) above SEIS (e), finalizing the installation (f). Images credit: NASA/JPL-Caltech

Geodesy provides constraints on the mass distribution within planets and, via the moment of inertia factor and the  $k_2$  Love number, gives estimates for the core size of Mars. These, however, also depend on assumptions on the mantle mineralogy and show a trade-off between core density and size, with best pre-landing estimates of the core radius between 1500 and 1900 km [11]. The measured  $k_2$  Love number indicates that the core of Mars is likely liquid. Uncertainties on properties of both mantle and core meant that it was also unclear at which depth phase transitions might occur in the mantle.

Estimates for seismic attenuation in the Martian interior were mostly based on extrapolations or conceptual models and mainly vary in the exponent used to describe the frequency-dependence of  $Q$  to relate constraints by the tidal period of the Martian moon Phobos to the seismic frequency band. In addition, mantle temperatures play an important role, meaning that  $Q$  might be larger than on Earth to a depth of about 300 km, but, due to higher temperatures, significantly smaller than on Earth at larger depths.

While it was assumed that Mars is seismically active, the level of this activity was uncertain by a factor of 10 [12, 13], and the seismically active regions on Mars could not be predicted with any confidence.

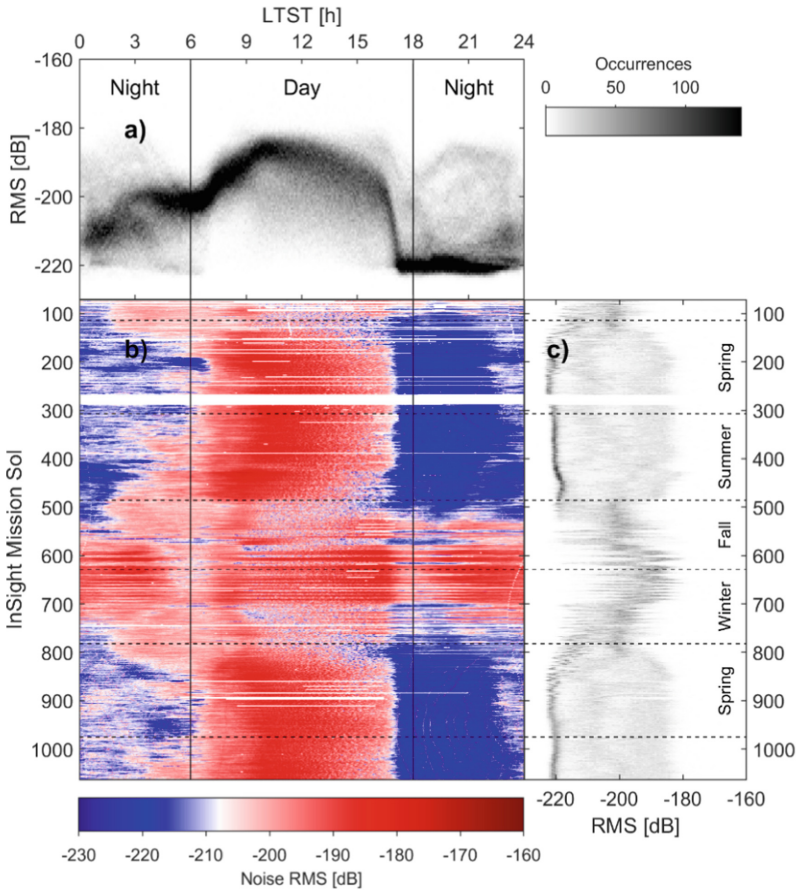
## 2 Seismic Environment of Mars

Due to the absence of oceans and anthropogenic activity, the background noise on Mars is mainly driven by the atmosphere. This results in a marked diurnal variation in the seismic noise level depending on wind conditions, with the highest noise level during the day linked to thermally-driven convective turbulence, and the lowest noise levels encountered in the evening after sunset, when activity in the thermal boundary layer is low [14–17]. Additionally, the prevailing wind directions and wind speeds change with season [18, 19], which leads to increased night-time noise levels in fall and winter (Fig. 2). Even during the windy periods, the background noise level between 0.1 and 0.6 Hz is low compared to Earth on all three components, i.e. below the New Low Noise Model [20], whereas during the quietest times, the instrument self-noise is detectable [21]. The low-noise evening and night-time is the primary period during which the weak marsquakes are detected with SEIS [15].

The atmosphere influences the noise level of SEIS in various ways, e.g. through direct forcing on the ground, mechanical vibrations of the lander structure at about 1.8 m distance from SEIS transferred through the shallow subsurface, and forcing on the WTS deployed over the seismometer and the tether linking SEIS to the lander (Fig. 1). Wind-induced vibrations of the lander lead to a number of narrow-band signals at frequencies above 1 Hz with amplitudes increasing with wind speed, and significantly larger on the horizontals than on the vertical component [15, 16, 22]. The peak frequencies of these lander modes are temperature-dependent. Besides, temporary modes linked to changes in the occupation – and hence position – of the IDA have also been documented [22]. They are distinct from a spectral line at 1 Hz and its multiples which is “tick-noise” caused by crosstalk of electrical signals within the tether related to temperature measurements performed once per second [16]. Additionally, resonances within the SEIS sensor assembly, i.e. related to the load shunt assembly on the SEIS tether, might also influence polarization measurements near the frequencies concerned, though they do not dominate the spectra [23]. At frequencies below 1 Hz, polarization analysis of the background noise shows a correlation of azimuth with wind direction variations, both diurnally and with season [21]. At frequencies above 0.3 Hz, the observed polarization along an inclined ellipse in the vertical plane can be explained by pressure waves propagating along the surface of Mars, or acoustic emissions from high altitudes in the atmosphere.

The large temperature variations of 80–100 K on the surface of Mars are the likely cause of a prominent disturbance in the SEIS data, the so-called glitches, which are one-sided pulses that can be modeled as instrument response to a step function in acceleration, often accompanied by high-frequency spikes that can be described by a simultaneous step functions in displacement [24]. The resulting signals affect all frequencies below 1 Hz and, due to amplitudes of up to  $10^{-7}$  m/s and more, cannot be ignored when analyzing seismic data in this frequency range. Though the SEIS installation reduces the daily temperature cycle directly affecting the instrument to about 15 K, most glitches can be attributed to thermal conductivity gradients and stresses between various parts of the sensor assembly. About a third of the glitches could be caused by actual rigid tilting of the SEIS instrument as a whole. Some glitches show repeating patterns over days, and occur at specific temperatures within the instrument, further pointing to a thermal

origin. Glitch sequences with stable time offsets that repeat every day [25] can strongly affect results of autocorrelation analyses, if not properly corrected for [26]. At higher frequencies above 10 Hz, short duration pulses of energy form another type of transient signal likely also related to temperature cycling on the lander, the tether, or SEIS, so-called “donks”, that are less predictable in timing and reproducible in signal shape, and thus harder to correct for, than glitches [16, 26].



**Fig. 2.** Daily and seasonal variations of the background noise level at SEIS. Noise amplitudes are given as displacement RMS computed over non-overlapping 2 min time windows, relative to 1m. a) Diurnal distribution of amplitudes, as count density, highlighting the day-night difference. b) Each line shows the RMS noise of one sol since the landing of InSight. The white point of the color scale is chosen such that blue regions correspond to times where the event amplitude distribution shows that the event catalog is representative. Data gap around sol 280 occurred during solar conjunction. c) Seasonal distribution of amplitudes, showing the increased noise during fall and winter.

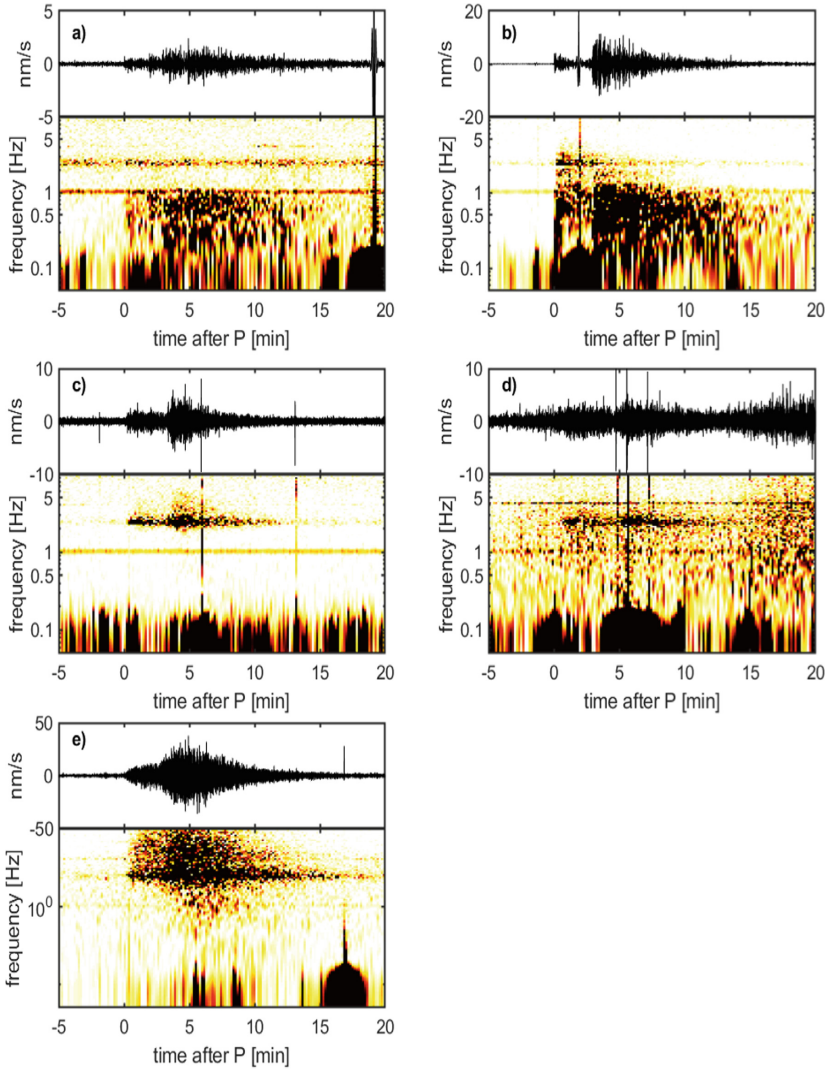
Another type of non-seismic transient signals is pressure drops associated with the passage of convective vortices (“dust devils”). They pull up the ground and thus create a tilt away from the vortex measurable with SEIS [27, 28]. Whereas these observations can be used to constrain the Young’s modulus of the ground (see Sect. 4.1), they also show up as broad-band non-seismic events in the SEIS data [16, 25].

### 3 Seismic Activity of Mars

Not surprising for a planet without plate tectonics, the seismicity of Mars is weak compared to Earth [27]. Only recently, after more than 900 sols of registration, the first events with moment magnitudes larger than 4.0 were detected [29]. The more than 1,300 smaller events recorded so far, however, provide a rich and valuable data set to study both the interior of Mars and its tectonics [30, 31]. Due to the extremely low night-time noise levels (see Sect. 2), marsquakes with moment magnitudes as small as 3.1 could be recorded and analyzed at distances of more than 3500 km, something impossible on Earth.

Based on their frequency content, marsquakes are sorted into two main groups (Fig. 3), the low frequency family, consisting of low-frequency (LF) and broad-band (BB) events, and the high frequency family, consisting of high-frequency (HF), very high frequency (VF) and 2.4 Hz events [15, 30].

LF and BB events, of which 90 have been identified in the data so far, dominantly contain energy below the 2.4 Hz resonance, with the BB events extending to (and sometimes above) 2.4 Hz, and usually contain two clear phases identified as P- and S-arrivals, similar to teleseismic earthquakes. Those events for which a stable backazimuth could be determined from the P-wave arrival have been located. The majority of available hypocenters are located about 1200 km to the northeast of InSight, at the giant fractures of the Cerberus Fossae region. This area of relatively recent volcanic activity had been postulated to be seismically active before the landing [32]. However, pre-landing models had also predicted seismic activity to be concentrated around Tharsis based on faults identified in orbital imagery and models of flexural loading, or, assuming global differential cooling of the lithosphere and thermal contraction as main cause of marsquakes, a rather homogeneous distribution [12]. The concentration of hypocenters in Cerberus Fossae now suggests recent tectonics as a major driver for marsquakes. Fault plane solutions for two of these events show normal faulting on fault planes with steep dips larger than  $75^\circ$ , indicating an extensional tectonic regime with an E-W to NE-SW orientation [33], in keeping with the interpretation of Cerberus Fossae as a graben system [32, 34]. For two atypical events of the LF family, with less pronounced P and S arrivals and persistent spectral peaks below 1 Hz, generation by a volcanic tremor-like mechanism has been investigated [35]. While it cannot be excluded, it would require low-viscosity magma and a high flux volume just within the inferred limits for Cerberus Fossae. The seismograms of the LF family events have been used to study the interior structure of Mars, from crustal layering to core size (see Sect. 4). While only events up to about  $100^\circ$  distance from InSight had been detected for most of the mission, two more recent events occurred at significantly larger distances, up to  $146^\circ$ , placing the source at Valles Marineris [29]. These more distant events within the core shadow zone allow to study the structure of the Martian mantle and core in more detail.



**Fig. 3.** VBB vertical component seismograms (top) and corresponding spectrograms (bottom) for five marsquakes, giving examples of the different event types. The spectrogram color axes are adapted to the respective event amplitudes. LF family seismograms are filtered between 0.1 and 1 Hz and HF family events between 0.25 and 8 Hz, respectively. a) LF event S0809a located at Cerberus Fossae. b) BB event S1133c, located at Cerberus Fossae. c) HF event S0490a. d) 2.4 Hz event S1045a. e) VF event S0794a. Prominent vertical lines in the spectrograms (and waveforms) are glitches; horizontal lines indicate tick noise at 1 Hz, the 2.4 Hz mode, and lander modes. Further event information is given in the Mars seismic catalog [31].



HF family events are dominated by energy at 2.4 Hz and above [30]. The most ubiquitous event type are the 2.4 Hz events, making up about three quarters of all detected events. They are characterized by an amplitude increase centered around the 2.4 Hz resonance, and little excitation above and below, and are likely weak HF events [36]. HF events predominantly show energy at 2.4 Hz and above, with limited energy below. VF events are special in that they extend to higher frequencies and contain significantly more energy on the horizontal components than on the vertical. HF and VF events often show two separate broad arrivals of seismic energy that have been interpreted as crustal P and S phases [15, 36]. In their frequency content, duration and signal shape, the event recordings are distinct from both earth- and moonquake seismograms, but can be modeled by the propagation of guided waves within the Martian crust that contains a very heterogeneous, scattering layer at the top [36]. Depending on the velocities assumed for these guided waves, the majority of HF events might also originate near Cerberus Fossae, whereas the VF events show no clear spatial clustering and occur over a wide range of distances. The occurrence of HF events shows a temporal pattern that is not an artefact of the variable detection efficiency due to the changing noise level [37]. Possible causes are solar illumination, the CO<sub>2</sub> ice evaporation cycle of Mars, or annual solar tides, which HF observations from a second Martian year will hopefully help to constrain further.

A final class of seismic events recorded by SEIS are super high frequency (SF) events, which only last for about 20 s, have energy at frequencies between 5 and 30 Hz, and occur in repeatable patterns [38]. Since the majority of the events occurs within  $\pm 2$  h of sunset and close to, but not at, the lander, their suggested origin is thermal cracking, similar to thermal events observed on the Moon.

## 4 Interior Structure of Mars

### 4.1 Shallow Subsurface

Geological interpretation of orbital data, available measurements from the Moon and Earth and laboratory experiments resulted in detailed expectations for the properties of the shallow-most part of the subsurface at InSight [39, 40]. Comparing those to direct in-situ measurements is important to improve the predictions from orbital constraints elsewhere on Mars, where they may be the only data available to assess trafficability and suitability for landing instruments or astronauts. Besides, low-velocity near-surface layers as expected on Mars due to the regolith cover can have an important influence on seismic recordings, and a better understanding of the elastic properties of the subsurface will also help to enlighten the penetration failure of InSight's heat flow probe HP<sup>3</sup> (Heat Flow and Physical Properties Package).

First constraints on the shallow sub-surface of the InSight landing site have been derived from an active seismic experiment: SEIS recorded the hammering of the unfortunate HP<sup>3</sup> experiment. The timing of the recordings could be used to determine the P-wave velocity of the regolith between HP<sup>3</sup> and SEIS to  $118 \pm 34$  m/s [14, 41], consistent with unconsolidated, cohesionless sand.

Information on larger depths could be derived from the recordings of the passage of convective vortices both with InSight's pressure sensor and SEIS by compliance analysis [27, 28, 42]. Those data allow to estimate the Young's modulus and its variation with depth down to about 20 m and find a strong increase in the values consistent with a discontinuity between the regolith and a stiffer layer at a depth between 0.7 and 7 m. Based on pre-landing models, the deeper layer is interpreted as blocky ejecta. With plausible assumptions on the density and Poisson's ratio, the inverted Young's moduli can be converted to P-wave velocities, which lie in the range of 136–152 m/s for the regolith layer, slightly higher than the values derived by hammering. However, these values integrate over the whole regolith layer and over larger distances from SEIS (i.e. over the ground properties up to the distance of the convective vortex when passing InSight) compared to the HP<sup>3</sup> measurements.

Analysis of horizontal-to-vertical spectral ratios of the ambient wavefield in the frequency range between 1.5 and 8 Hz has been used to constrain the subsurface structure to around 200 m depth [43]. The main feature in this frequency range is the 2.4 Hz mode that results in a trough in the H/V curve and can be explained by a low-velocity layer, something that was not predicted prior to landing [44]. Inversion places this layer at 30 to 75 m depth, with the layers above and below interpreted as Hesperian and Amazonian basalts and the low-velocity layer as sediments deposited between those lava flows. Ongoing analysis over a broader frequency range using seismic event coda will refine these results [45].

Temporal variations in the elastic properties of the shallow subsurface have also been studied using both coda wave interferometry of SF events and passive image interferometry of the background wavefield [46]. The measured velocity perturbations can be explained by the thermoelastic response of the shallow subsurface, down to about 20 m depth, to the seasonally variable solar insolation, where the spatial and temporal variations of the surface temperature induce stresses in the subsurface that lead to changes in the seismic velocities.

## 4.2 Crust

Much of the Martian crust formed relatively early during the planet's history during widespread melting, with incompatible elements, such as radioactive elements and volatiles, concentrating in the melt. These elements are accordingly sequestered in the crust, with consequences for the thermal and magmatic evolution of Mars. Models for the chemical composition of the Martian crust are generally based on orbital data that are at best sensitive to the upper few kilometers of the planet, and sometimes only to centimeters or micrometers. Extrapolating these data to the whole crust might thus be misleading. Besides, large uncertainties on the average crustal thickness of Mars remained before InSight (see Sect. 1.2).

Mars' crustal thickness and layering was primarily investigated using two methods, either based on waves converted from P to S or vice versa at discontinuities in the elastic properties beneath the landing site and extracted via the calculation of receiver functions [14, 47, 48], or based on reflections of P-waves derived from ambient vibration autocorrelations [47, 49, 50]. P-to-S receiver functions of the first few events showed three prominent onsets within the first 8 s, something that has in the meantime been

confirmed using more data. Since a majority of events is located at Cerberus Fossae (see 3), identifying any move-out of the phases has been difficult so far. This inhibits the interpretation of the data since the primary arrival from a third discontinuity at depth could be hidden below a multiply reflected and converted phase of the first layer arriving at the same time [47]. Analysis of additional events as well as modeling of the S-to-P receiver function of one event strongly favors the interpretation with three layers [48], whereas autocorrelations are unable to distinguish between the two models.

Independent of the interpretation of the third signal, the crust shows rather low seismic velocities. The top-most layer extends to a depth of  $8 \pm 2$  km and has S-wave velocities below 2 km/s. Recently, SH-reflections within this layer have also been identified [51]. They require lower velocities to explain their timing than the P-SV conversions, thus pointing to radial anisotropy in the upper-most layer that might be caused by cracks or inclusions. The observed low velocities cannot be reconciled with pristine basalt, but require damaged or altered material. Rock physics models show that the observed velocities are too low for ice-saturated cracks, excluding a cryosphere confining an aquifer at depth below InSight [52]. Beneath the top layer, S-velocities increase to around 2.6 km/s in a layer down to  $20 \pm 5$  km depth [47]. These velocities could be explained by cemented pore space [52]. A third crustal layer would show only a slight velocity contrast to the mantle, with S-wave velocities of 2.8 to 3.5 km/s to  $39 \pm 8$  km.

Due to the nature of the wave phases studied here, the results only image the crustal structure in the vicinity of the InSight lander. Gravity and topography allow to extend this point measurements to map the crustal thickness across all of Mars. Including the measurement uncertainties, this results – for the thicker, more likely crustal model – in a global average crustal thickness of 39 to 72 km, and 24 to 38 km for the thinner, two layer model. This is thinner than some of the previous predictions, and also means that the bulk crustal density has to be less than  $3100 \text{ kg m}^{-3}$  [47], which requires porosity, fractures or the existence of felsic rocks within the crust not represented by surficial measurements from the orbiter [58]. However, only additional observations, e.g. from surface waves, could help to understand if the observed layering is ubiquitous. In addition, geodynamic and geologic modeling indicate that the crustal models require an enrichment in radioactive elements by a factor of 13 to 21 compared to the primitive mantle [47, 53], which is more than what is expected based on orbital gamma-ray mapping of the near surface and indicates that the near surface might not be representative of the whole crust.

Another important property of the crust, attenuation, has been investigated by studying the energy decay in seismogram envelopes [36, 54, 55]. The envelope shapes of HF and VF events have been modeled by diffusion [54] and by an elastic radiative transfer approach [55]. A diffusion model cannot explain the envelope shapes of the LF family events, though, and scattering strength accordingly has to decrease with depth [54]. The upper-most crustal layer could thus be highly heterogeneous and support multiple scattering, similar to what is observed on the Moon, although within a megaregolith of much greater depth. Furthermore, attenuation is very low on Mars, indicating a mostly dry medium along the propagation path of the HF family events [55].

### 4.3 Mantle

The mantle of Mars to a depth of about 800 km has been investigated with the help of surface-reflected phases, i.e. PP, PPP, SS and SSS [53], whereas information on deeper structure so far relies on ScS phases [56]. A weakly negative S-velocity gradient in the mantle indicates a lithosphere of more than 400 km thickness, consistent with a large thermal gradient across the lithosphere of a stagnant-lid planet, and leads to a weak S-wave shadow zone at epicentral distances between 40° and 60°.

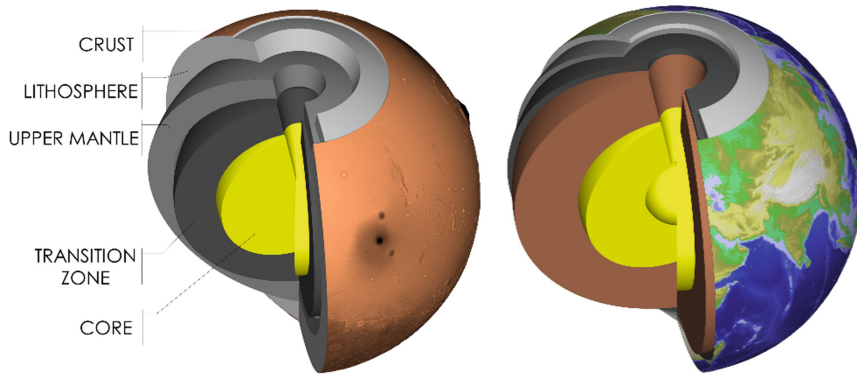
Observations and modeling of triplicated phases from LF family marsquakes at 60° to 85° epicentral distance have been used to constrain the top of the mantle transition zone defined by the olivine-to-wadsleyite phase transition, finding a Martian mantle colder than pre-mission estimates and a broader transition compared to Earth, consistent with a more iron-rich mantle [57]. The phase transition to bridgemanite in the Martian mantle is prevented by the size of the core (see Sect. 4.4).

### 4.4 Core

The observation of ScS phases constrains the size of the core to  $1830 \pm 40$  km [56], at the larger end of the previously assumed range. While the comparatively large amplitudes of the reflected phases confirm a fluid state of the core, its large size requires a rather low density, in the range of 5.7 to 6.3  $\text{g cm}^{-3}$ . This means that a substantial amount of light elements, e.g. C, O and H, in addition to sulfur, is contained in the core, making it different in composition from the Earth's core. Furthermore, the absence of an insulating bridgemanite layer in the mantle allowed a higher heat flux from the core as compared to Earth early in the history of the planet, which – via a thermally driven dynamo – could explain the observed crustal magnetism in the absence of a present-day magnetic field.

## 5 Conclusions

As was the case with Apollo for the Moon, bringing seismology to Mars has resulted in observing waveforms distinct from those known on Earth (HF family events), and new types of phenomena (temporal variability in HF event occurrence). The exceptionally low noise level on Mars has enabled us to use rather small quakes to get a first seismic model of the interior structure, once again highlighting differences from Earth (Fig. 4), i.e. a thick lithosphere, a S-wave shadow zone around 50° distance, no lower mantle, and a large, light core. InSight is still gathering more data, and the analysis of previous data and their meaning is an ongoing effort. We can thus hope to answer more questions – and make new observations that challenge our current understanding of Mars and the formation and evolution of terrestrial planets – with this remarkable mission.



**Fig. 4.** Simplified interior structure of Mars, in comparison to Earth. Crustal thickness, lithosphere, mantle transition zone and core size of Mars are taken from [47, 53, 56]. Corresponding layers in Earth and Mars share the same color. The 660 km discontinuity in Earth, and the lower mantle (brown), have no counterpart in Mars. The absence of an inner core in Mars is widely presumed, but not yet proven. Topography is stretched by a factor of five on both planets; surface colors show elevation in both cases, but try to resemble true surface colors. The actual size of Mars is about the same as the size of Earth's core.

**Acknowledgements.** This is InSight Contribution Number (ICN) 262. We acknowledge NASA, CNES, their partner agencies and institutions (UKSA, SSO, DLR, JPL, IPGP-CNRS, ETHZ, IC, and MPS-MPG), and the flight operations team at JPL, SISMOC, MSDS, IRIS-DMC, and PDS for providing SEED SEIS data. InSight SEIS data are available from the IPGP Data Center, IRIS-DMC, and NASA PDS (InSight Mars SEIS Data Service: SEIS raw data, InSight Mission. IPGP, JPL, CNES, ETHZ, ICL, MPS, ISAE-Supaero, LPG, MSFC (2019), [https://doi.org/10.18715/SEIS.INSIGHT.XB\\_2016](https://doi.org/10.18715/SEIS.INSIGHT.XB_2016)).

## References

1. Hall, R.C.: Lunar impact - a history of project ranger. NASA SP-4210. NASA Scientific and Technical Information Office (1977)
2. Nakamura, Y., Latham, G.V., Dorman, H.J.: Apollo lunar seismic experiment - final summary. *J. Geophys. Res.* **87**, A117–A123 (1982)
3. Lammlein, D.R., Latham, G.V., Dorman, J., Nakamura, Y., Ewing, M.: Lunar seismicity, structure, and tectonics. *Rev. Geophys.* **12**(1), 1–21 (1974)
4. Garcia, R.F., et al.: Lunar seismology: an update on interior structure models. *Space Sci. Rev.* **215**(8), 1–47 (2019)
5. Anderson, D.L., Miller, W.F., Latham, G.V., Nakamura, Y., Toksöz, M.N., Dainty, et al.: Seismology on Mars. *J. Geophys. Res.* **82**(28), 4524–4546 (1977)
6. Nakamura, Y., Anderson, D.L.: Martian wind activity detected by a seismometer at Viking Lander 2 site. *Geophys. Res. Lett.* **6**(6), 499–502 (1979)
7. Panning, M.P., Pike, W.T., Lognonné, P., Banerdt, W.B., Murdoch, N., Banfield, D., et al.: On-deck seismology: Lessons from InSight for future planetary seismology. *J. Geophys. Res.: Planets* **125**(4), e2019JE006353 (2020)

8. Lognonné, P., Banerdt, W.B., Giardini, D., Pike, W.T., Christensen, U., Laudet, P., et al.: SEIS: InSight's seismic experiment for internal structure of Mars. *Space Sci. Rev.* **215**(1), 1–170 (2019). <https://doi.org/10.1007/s11214-018-0574-6>
9. Cole, G.H.A.: The internal structure of planetary bodies. *Contemp. Phys.* **13**(6), 585–600 (1972)
10. Smrekar, S.E., et al.: Pre-mission insights on the interior of Mars. *Space Sci. Rev.* **215**(1), 1–72 (2018). <https://doi.org/10.1007/s11214-018-0563-9>
11. Knapmeyer, M., Walterova, M.: Planetary Core Radii: From Plato towards PLATO. submitted to *Advances in Geophysics* (2022)
12. Knapmeyer, M., Oberst, J., Hauber, E., Wählisch, M., Deuchler, C., Wagner, R.: Working models for spatial distribution and level of Mars' seismicity. *J. Geophys. Res.: Planets* **111**, E11006 (2006)
13. Plesa, A.-C., Knapmeyer, M., Golombek, M.P., Breuer, D., Grott, M., Kawamura, T., et al.: Present-day Mars' seismicity predicted from 3-D thermal evolution models of interior dynamics. *Geophys. Res. Lett.* **45**, 2580–2589 (2018)
14. Lognonné, P., Banerdt, W.B., Pike, W.T., Giardini, D., Christensen, U., Garcia, R.F., et al.: Constraints on the shallow elastic and anelastic structure of Mars from InSight seismic data. *Nat. Geosci.* **13**, 213–220 (2020)
15. Giardini, D., Lognonné, P., Banerdt, W.B., Pike, W.T., Christensen, U., Ceylan, S., et al.: The seismicity of Mars. *Nat. Geosci.* **13**(3), 205–212 (2020)
16. Ceylan, S., Clinton, J., Giardini, D., Boese, M., Charalambous, C., van Driel, M., et al.: Companion guide to the Marsquake Catalog from InSight, Sols 0–478: data content and non-seismic events. *Phys. Earth Planet. Inter.* **310**, 106597 (2021)
17. Banfield, D., et al.: The atmosphere of Mars as observed by InSight. *Nat. Geosci.* **13**, 190–198 (2020)
18. Spiga, A., Murdoch, N., Lorenz, R., Forget, F., Newman, C., Rodriguez, S., et al.: A study of daytime convective vortices and turbulence in the Martian planetary boundary layer based on half-a-year of InSight atmospheric measurements and large-eddy simulations. *J. Geophys. Res.: Planets* **126**(1), e2020JE006511 (2021)
19. Charalambous, C., Stott, A.E., Pike, W.T., McClean, J.B., Warren, T., Spiga, A., et al.: A comodulation analysis of atmospheric energy injection into the ground motion at InSight, Mars. *J. Geophysical Res.: Planets* **126**, e2020JE006538 (2021)
20. Peterson, J.R.: Observations and modeling of seismic background noise. U.S. Geological Survey Open-File Report 93–322, USGS Publications Warehouse (1993)
21. Stutzmann, E., Schimmel, M., Lognonné, P., Horleston, A., Ceylan, S., van Driel, M., et al.: The polarization of ambient noise on Mars. *J. Geophys. Res.: Planets* **126**, e2020JE006545 (2021)
22. Dahmen, N.L., Zenhäusern, G., Clinton, J.F., Giardini, D., Stähler, S.C., Ceylan, S., et al.: Resonances and lander modes observed by InSight on Mars (1–9 Hz). *Bull. Seismol. Soc. Am.* **111**(6), 2924–2950 (2021)
23. Hurst, K., Fayon, L., Knapmeyer-Endrun, B., Schmelzbach, C., van Driel, M., Ervin, J., et al.: Resonances of the InSight seismometer on Mars. *Bull. Seismol. Soc. Am.* **111**(6), 2951–2963 (2021)
24. Scholz, J.-R., Widmer-Schmidrig, R., Davis, P., Lognonné, P., Pinot, B., Garcia, R.F., et al.: Detection, analysis, and removal of glitches from InSight's seismic data from Mars. *Earth and Space Sci.* **7**, e2020EA001317 (2020)
25. Barkaoui, S., Lognonné, P., Kawamura, T., Stutzmann, E., Seydoux, L., de Hoop, M.V., et al.: Anatomy of continuous Mars SEIS and pressure data from unsupervised learning. *Bull. Seismol. Soc. Am.* **111**(6), 2964–2981 (2021)

26. Kim, D., Davis, P., Lekić, V., Maguire, R., Compaire, N., Schimmel, M., et al.: Potential pitfalls in the analysis and structural interpretation of seismic data from the Mars InSight mission. *Bull. Seismol. Soc. Am.* **111**(6), 2982–3002 (2021)
27. Banerdt, W.B., Smrekar, S.E., Banfield, D., Giardini, D., Golombek, M., Johnson, C.L., et al.: Initial results from the InSight mission on Mars. *Nat. Geosci.* **13**(3), 183–189 (2020)
28. Murdoch, N., Spiga, A., Lorenz, R., Garcia, R.F., Perrin, C., Widmer-Schmidrig, R., et al.: Constraining Martian regolith and vortex parameters from combined seismic and meteorological measurements. *J. Geophys. Res.: Planets* **126**(2), e2020JE006410 (2021)
29. Horleston, A., Clinton, J.F., Ceylan, S., Giardini, D., Charalambous, C., Irving, J.C.E., et al.: The far side of Mars: two distant marsquakes detected by InSight. *The Seismic Rec.* **2**(2), 88–99 (2022)
30. Clinton, J., Ceylan, S., van Driel, M., Giardini, D., Stähler, S.C., Böse, M., et al.: The marsquake catalog from InSight, Sols 0–478: data content and non-seismic events. *Phys. Earth Planet. Inter.* **310**, 106595 (2021)
31. InSight Marsquake Service: Mars Seismic Catalogue, InSight Mission; V9 2022–01–01. ETHZ, IGP, JPL, ICL, Univ. Bristol. <https://doi.org/10.12686/a14>
32. Taylor, J., Teanby, N. A., Wookey, J.: Estimates of seismic activity in the Cerberus Fossae region of Mars. *J. Geophysical Res.: Planets* **118**, 2570–2581 (2013)
33. Brinkman, N., Stähler, S.C., Giardini, D., Schmelzbach, C., Khan, A., Jacob, A., et al.: First focal mechanisms of marsquakes. *J. Geophysical Res.: Planets* **126**(4), e2020JE006546 (2021)
34. Perrin, C., Jacob, A., Lucas, A., Myhill, R., Hauber, E., Batov, A., et al.: Geometry and segmentation of Cerberus Fossae, Mars: Implications for marsquake properties. *J. Geophysical Res.: Planets* **127**, e2021JE007118 (2022)
35. Kedar, S., Panning, M.P., Smrekar, S.E., Stähler, S.C., King, S.D., Golombek, M.P., et al.: Analyzing low frequency seismic events at Cerberus Fossae as long period volcanic quakes. *J. Geophysical Res.: Planets* **126**(4), e2020JE006518 (2021)
36. van Driel, M., Ceylan, S., Clinton, J.F., Giardini, D., Horleston, A., Margerin, L., et al.: High-frequency seismic events on Mars observed by InSight. *J. Geophysical Res.: Planets* **126**(2), e2020JE006670 (2021)
37. Knapmeyer, M., Stähler, S.C., Daubar, I., Forget, F., Spiga, A., Pierron, T., et al.: Seasonal seismic activity on Mars. *Earth Planet. Sci. Lett.* **576**, 117171 (2021)
38. Dahmen, N.L., Clinton, J.F., Ceylan, S., van Driel, M., Giardini, D., Khan, A., et al.: Super high frequency events: a new class of events recorded by the InSight seismometers on Mars. *J. Geophysical Res.: Planets* **126**(2), e2020JE006599 (2021)
39. Morgan, P., et al.: A pre-landing assessment of regolith properties at the InSight landing site. *Space Sci. Rev.* **214**(6), 1–47 (2018). <https://doi.org/10.1007/s11214-018-0537-y>
40. Golombek, M., et al.: Geology and physical properties investigations by the InSight lander. *Space Sci. Rev.* **214**(5), 1–52 (2018). <https://doi.org/10.1007/s11214-018-0512-7>
41. Brinkman, N., Schmelzbach, C., Sollberger, D., van Driel, M., ten Pierick, J., Robertsson, J.O.A. et al.: The first active seismic experiment on Mars to characterize the shallow subsurface structure at the InSight landing site. *SEG Technical Program Expanded Abstracts*, pp. 4756–4760 (2019)
42. Kenda, B., Drilleau, M., Garcia, R.F., Kawamura, T., Murdoch, N., Compaire, N., et al.: Subsurface structure at the InSight landing site from compliance measurements by seismic and meteorological experiments. *J. Geophysical Res.: Planets* **125**(6), e2020JE006387 (2020)
43. Hobiger, M., Hallo, M., Schmelzbach, C., Stähler, S.C., Fäh, D., Giardini, D., et al.: The shallow structure of Mars at the InSight landing site from inversion of ambient vibrations. *Nature Commun.* **12**, 6756 (2021)
44. Knapmeyer-Endrun, B., et al.: Influence of body waves, instrumentation resonances, and prior assumptions on rayleigh wave ellipticity inversion for shallow structure at the InSight landing site. *Space Sci. Rev.* **214**(5), 1–42 (2018). <https://doi.org/10.1007/s11214-018-0529-y>

45. Carrasco, S., et al.: Empirical H/V spectral ratios at the InSight landing site and implications for martian subsurface structure. *Geophys. J. Int.* (2022). under review
46. Compaire, N., Margerin, L., Monnerneau, M., Garcia, R.F., Lange, L., Calvet, M., et al.: Seasonal variations of subsurface seismic velocities monitored by the SEIS-InSight seismometer on Mars. *Geophys. J. Int.* **229**(2), 776–799 (2022)
47. Knapmeyer-Endrun, B., Panning, M.P., Bissig, F., Joshi, R., Khan, A., Kim, D., et al.: Thickness and structure of the martian crust from InSight seismic data. *Science* **373**(6553), 438–443 (2021)
48. Kim, D., Lekić, V., Irving, J.C.E., Schmerr, N., Knapmeyer-Endrun, B., Joshi, R., et al.: Improving constraints on planetary interiors with PPs receiver functions. *J. Geophysical Res.: Planets* **126**(11), e2021JE006983 (2021)
49. Compaire, N., Margerin, L., Garcia, R.F., Pinot, B., Calvet, M., Orhand-Mainsant, G. et al.: Autocorrelation of the ground vibrations recorded by the SEIS-InSight seismometer on Mars. *J. Geophysical Res.: Planets* **126**(4), e2020JE006498 (2021)
50. Schimmel, M., Stutzmann, E., Lognonné, P., Compaire, N., Davis, P., Drilleau, M., et al.: Seismic noise autocorrelations on Mars. *Earth and Space Science* **8**(6), e2021EA001755 (2021)
51. Li, J., Beghein, C., Wookey, J., Davis, P., Lognonné, P., Schimmel, M., et al.: Evidence for crustal seismic anisotropy at the InSight landing site. *Earth Planet. Sci. Lett.* **593**, 117654 (2022)
52. Manga, M., Wright, V.: No cryosphere-confined aquifer below InSight on Mars. *Geophysical Res. Letters* **48**(8), e2021GL093127 (2021)
53. Khan, A., Ceylan, S., van Driel, M., Giardini, D., Lognonné, P., Samuel, H., et al.: Upper mantle structure of Mars from InSight seismic data. *Science* **373**(6553), 434–438 (2021)
54. Karakostas, F., Schmerr, N., Maguire, R., Huang, Q., Kim, D., Lekić, V., et al.: Scattering attenuation of the martian interior through coda-wave analysis. *Bull. Seismol. Soc. Am.* **111**(6), 3035–3054 (2021)
55. Menina, S., Margerin, L., Kawamura, T., Lognonné, P., Marti, J., Drilleau, M., et al.: Energy envelope and attenuation characteristics of high-frequency (HF) and very-high-frequency (VF) martian events. *Bull. Seismol. Soc. Am.* **111**(6), 3016–3034 (2021)
56. Stähler, S.C., Khan, A., Banerdt, W.B., Lognonné, P., Giardini, D., Ceylan, S., et al.: Seismic detection of the martian core. *Science* **373**(6553), 443–448 (2021)
57. Huang, Q., Schmerr, N.C., King, S.D., Rivoldini, A., Plesa, A.-C., Samuel, H., et al.: Constraints on the depth of the martian mantle transition zone from triplicated waveforms. In: 53<sup>rd</sup> Lunar and Planetary Science Conference, 1673, Woodlands, Texas (2022)
58. Wieczorek, M., et al.: InSight constraints on the global character of the martian crust. *J. Geophys. Res.: Planets* **127**, e2022JE007298 (2022)